

# Probing Neural TSP Representations for Prescriptive Decision Support

Reuben Narad<sup>1</sup> Léonard Boussioux<sup>1,2</sup> Michael Wagner<sup>1</sup>

## Abstract

The field of neural combinatorial optimization (NCO) trains neural policies to solve NP-hard problems such as the traveling salesperson problem (TSP). We ask whether, beyond producing good tours, a trained TSP solver learns internal representations that transfer to other optimization-relevant objectives, in the spirit of transfer learning from other domains. We train several attention-based TSP policies, collect their internal activations, and train probes on node/edge embeddings for two NP-hard prescriptive downstream tasks inspired by real-world logistics scenarios: node-removal sensitivity (identifying the most impactful node to remove) and edge-forbid sensitivity (identifying the most critical edge to retain). On a Euclidean TSP100-trained model, probes for both tasks are competitive with existing baselines. Ensembling probe signals with geometric features outperforms the strongest baselines: 65% top-1 accuracy (vs. 58% baseline) for the best-node-removal task, and 73% top-1 accuracy (vs. 67% baseline) for the worst-edge identification task. To our knowledge, we are the first to study neural TSP solvers as transferable encoders for prescriptive what-if decision-support objectives beyond tour construction. Finally, we show that transfer accuracy increases with solver quality across training and model scale, suggesting that training stronger NCO solvers also yields more useful encoders for downstream objectives. Our code is available at: [github.com/ReubenNarad/tsp\\_prescriptive\\_probe](https://github.com/ReubenNarad/tsp_prescriptive_probe).

## 1. Introduction

Combinatorial optimization underlies core decisions in logistics, transportation, manufacturing, and networked sys-

<sup>1</sup>Foster School of Business, University of Washington, Seattle, WA, USA <sup>2</sup>Paul G. Allen School of Computer Science & Engineering, University of Washington, Seattle, WA, USA. Correspondence to: Reuben Narad <rnarad@uw.edu>.

Preprint. February 10, 2026.

tems, where small improvements in cost or latency translate directly into operational value. For many of these problems, classical operations-research (OR) methods provide strong performance, but often require substantial modeling effort and can be computationally heavy or difficult to adapt when constraints change. Motivated by the success of deep learning in other domains, *neural combinatorial optimization* (NCO) trains neural policies, typically with reinforcement learning, to directly construct solutions from problem instances (Vinyals et al., 2015; Bello et al., 2016; Kool et al., 2018; Nazari et al., 2018). These learned solvers can be extremely fast at inference and are attractive as flexible heuristics, but they frequently remain less reliable than highly optimized classical pipelines, especially under distribution shift or at larger scales (Bengio et al., 2018; Cappart et al., 2021; Joshi et al., 2020).

This paper argues that the value of training strong NCO solvers is not limited to using them as drop-in replacements for OR algorithms. In other areas of machine learning, models trained on a single objective often learn representations that transfer to many downstream tasks; for example, language models trained on next-token prediction produce embeddings useful for a wide range of linguistic objectives. We ask an analogous question for NCO: *do neural TSP solvers learn internal representations that encode actionable structure beyond tour construction, and does that structure strengthen as the solver improves?* Prior work has begun to probe and interpret NCO representations (Zhang et al., 2025a;b) and to extract human-interpretable features from solver activations (Narad et al., 2025), but the emphasis has largely been on characterization. Our focus is instead on *transfer to prescriptive, optimization-relevant objectives* and on establishing a systematic relationship between solver quality and representation usefulness.

To evaluate transfer, we introduce and formalize two downstream tasks on Euclidean TSP instances, chosen to be both practically motivated and expensive to solve exactly at scale. The first task is **node-removal sensitivity** (“which node, if removed, would most reduce the optimal tour length?”), which requires an optimal re-solve for each candidate removal to obtain ground-truth deltas. The second task is **edge-forbid sensitivity** (“which tour edge is most critical to retain?”), similarly requiring repeated optimal re-solves under edge constraints.

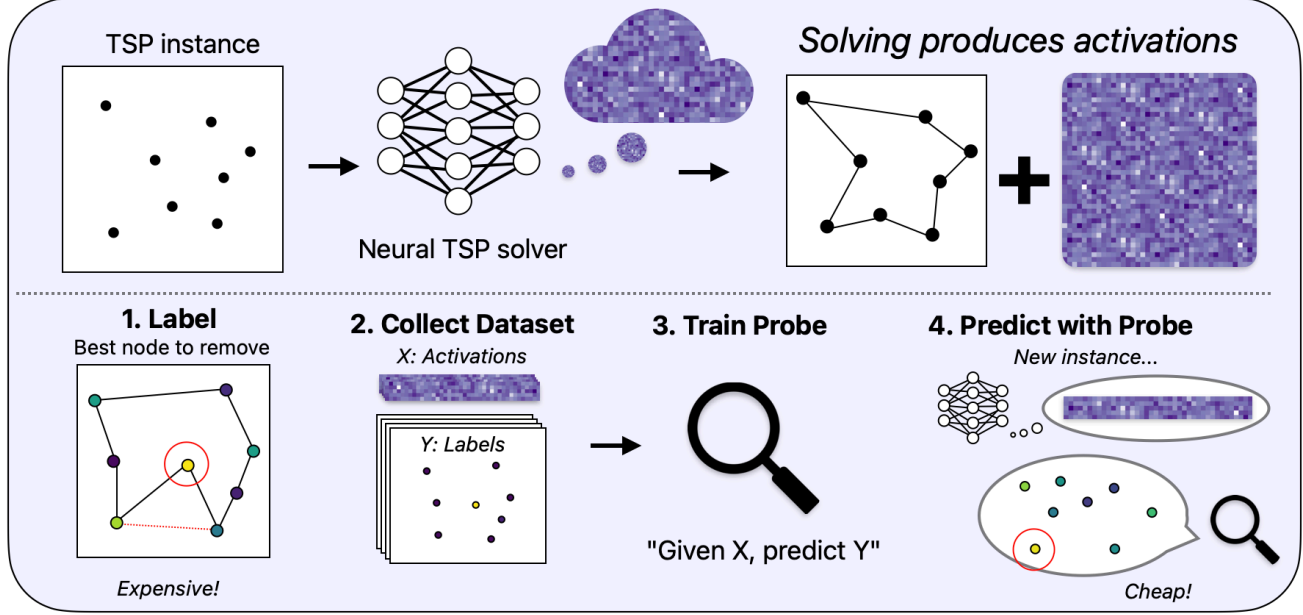


Figure 1. Overview of the probing pipeline. We train a neural TSP solver, extract frozen encoder node embeddings from a single forward pass, and generate sensitivity labels by repeatedly re-solving to optimality under small interventions (node-removal or tour-edge-forbiddance). We then train probes on cached representations to predict which node to remove or which tour edge is most critical to retain.

**Usage setting and information available at query time.** The two sensitivity tasks correspond to different decision-support settings. Node-removal is a *pre-solve* advisory query (e.g., deciding which stop to drop before committing to a full solve), so we evaluate methods that operate on the instance geometry alone without requiring a tour. Edge-forbid is a *post-solve* contingency query (e.g., a road closure on a planned route), so we assume a base tour is already available and restrict candidates to edges on that tour; edges not on the base tour are irrelevant under our optimality-gap label definition.

Across these tasks, the appeal of representation-based predictors is that they can be orders of magnitude cheaper than repeated exact solves, while still providing useful rankings and decision support. Figure 1 illustrates our overall approach: we train a neural TSP solver, extract frozen encoder representations, generate sensitivity labels via repeated optimal re-solves, and train probes to predict sensitivity rankings for new instances.

Our experimental setup is deliberately simple. We train an attention-based TSP policy in the style of (Kool et al., 2018) using RL4CO (Berto et al., 2023), sweeping model scale (three sizes) and collecting checkpoints throughout training. For each task, we construct labeled datasets of thousands of TSP instances (task-dependent), and for each instance we extract frozen internal activations from the solver encoder. We then train a family of probes on these activations alone, ranging from linear models to permutation-invariant set-based decoders (DeepSets (Zaheer et al., 2017) and Set

Transformers (Lee et al., 2019)), and compare against non-representation baselines that use only instance geometry or heuristic features.

We find that trained solver representations contain non-trivial, actionable signal: probes on frozen activations are strong relative to geometry-based baselines, and adding probe signal via ensembling improves the strongest baseline under comparable constraints; performance also improves substantially over probes trained on untrained model representations. Crucially, representation usefulness tracks solver quality. Across checkpoints within a single run, probes become more accurate as the policy improves, and across model sizes, larger/better solvers yield more transferable representations on the same downstream tasks. Notably, in our training dynamics, probe accuracy can continue to improve even after tour-cost improvements largely plateau, suggesting that representation learning continues beyond what is visible in standard solver metrics.

In summary, this work makes three contributions. First, we formalize two prescriptive downstream tasks for probing NCO representations, centered on sensitivity. Second, we provide an evaluation pipeline for extracting frozen solver activations and training controlled probe families under strong non-representation baselines. Third, we empirically demonstrate that (i) neural TSP solver representations transfer to these downstream objectives and (ii) transfer strength correlates with solver quality across training and scale, suggesting that improvements to NCO solvers can yield dividends beyond solution quality by producing more

useful representations for downstream decision support.

The remainder of the paper introduces the tasks and probing methodology, describes datasets and training details, and presents main transfer results together with training-dynamics and scaling analyses.

## 2. Related Work

**Neural combinatorial optimization** A growing body of work trains neural policies to solve NP-hard combinatorial optimization problems, including routing, via pointer-network style architectures and reinforcement learning (Vinyals et al., 2015; Bello et al., 2016; Kool et al., 2018; Nazari et al., 2018). Modern routing solvers include stronger training/decode schemes such as POMO (Kwon et al., 2020), and iterative/improvement-style approaches that refine solutions or guide local search (e.g., DACT and learned-guided local search) (Ma et al., 2021; Hudson et al., 2021). Benchmarks and libraries such as RL4CO help standardize evaluation across many CO environments and baselines (Berto et al., 2023). For broader context and evaluation methodology, see surveys and generalization analyses (Bengio et al., 2018; Joshi et al., 2020; Cappart et al., 2021).

**Probing and interpretability.** Probing is a technique for analyzing what information is encoded in learned representations: given a pretrained model, we freeze its representations and train a separate classifier or regressor (the “probe”) to predict a target property from those frozen features. The probe’s accuracy reveals whether the target signal is accessible in the representations, while controlling probe capacity helps distinguish information that is explicitly encoded from information that could be recovered through complex non-linear decoding (Hewitt & Manning, 2019; Hewitt & Liang, 2019). In neural combinatorial optimization, (Zhang et al., 2025a) study NCO representations through probing tasks and introduce coefficient-significance probing (CS-Probing) (Zhang et al., 2025b). Complementary mechanistic analyses use sparse autoencoders to extract interpretable latent features from neural TSP solvers (Narad et al., 2025).

**Foundation and generalist models for routing.** Recent work has begun to frame neural routing solvers as *foundation* or *generalist* models: a single trained model is expected to represent and solve many VRP variants by conditioning on task attributes and sharing internal representations across problem types. RouteFinder introduces a unified VRP environment and a transformer model with global attribute embeddings and adapters, trained across dozens of VRP variants with mixed-batch multi-task RL (Berto et al., 2024). Related efforts also unify multiple routing problems via compositional attribute representations and evaluate zero-shot generalization to unseen attribute combinations (Liu

et al., 2024), and increase capacity for multi-variant solving via mixture-of-experts architectures (Zhou et al., 2024), with recent extensions incorporating distributional shift across real-world maps (Goh et al., 2025). These works primarily target *solution quality* across diverse routing constraints. Our focus is complementary: we treat a trained solver as a transferable *encoder* and study whether its representations support *prescriptive decision-support* queries (sensitivity and what-if ranking) beyond constructing tours.

**Sensitivity, interdiction, and what-if objectives.** Sensitivity and interdiction problems are classical in OR: they ask how solutions change under perturbations (sensitivity) or adversarial constraints (interdiction). Recent work has begun applying learning-based methods to these problems, including learned advisory signals for network interdiction (Zhang et al., 2024) and deep sensitivity analysis methods for objective-oriented combinatorial optimization (Gireesan et al., 2024). For TSP, interdiction and fortification formulations have been studied in the classical OR literature (Lozano et al., 2017), while local-search heuristics such as 2-opt and Lin–Kernighan (Croes, 1958; Lin & Kernighan, 1973) provide standard repair baselines when tour edges must be modified. Our work differs by using learned TSP solver representations to predict sensitivity rankings, rather than computing them via re-optimization or local search.

**Pretraining and learning-augmented algorithms.** Beyond end-to-end neural solvers, learning can also be integrated into classical algorithms. Learning-augmented approaches incorporate learned signals into combinatorial algorithms to guide search and improve generalization (Li et al., 2025), while graph-pretraining for combinatorial optimization (Yuan et al., 2025). Our work is complementary: we study whether representations from a trained TSP solver transfer to related decision-support objectives.

## 3. Methodology

### 3.1. Problem Setup and Notation

We study TSP instances with  $n$  nodes and coordinates  $X = \{x_i\}_{i=1}^n$ ,  $x_i \in \mathbb{R}^2$ . In our main setting, nodes are sampled uniformly from  $[0, 1]^2$ . A tour is a permutation  $\pi$  of  $\{1, \dots, n\}$  with length  $L(\pi; X) = \sum_{t=1}^n d(\pi_t, \pi_{t+1})$  where  $\pi_{n+1} = \pi_1$ . For ground-truth labels, we compute optimal tour lengths using Concorde (Applegate et al., 2006), a state-of-the-art exact TSP solver. To match Concorde’s coordinate-based input format, we scale coordinates by 100, round to 4 decimals, and compute distances as  $d(i, j) = \|x_i - x_j\|_2$  on the scaled coordinates.

The optimal length is  $L^*(X) = \min_{\pi} L(\pi; X)$ , obtained via Concorde for each instance.

We denote the trained TSP policy by  $\pi_\theta$  and its encoder by  $f_\theta$ . Given an instance, the encoder produces node embeddings  $H = f_\theta(X) = \{h_i\}_{i=1}^n$ ,  $h_i \in \mathbb{R}^d$ . We freeze  $f_\theta$  and use  $\{h_i\}$  as representations for downstream prediction. Downstream tasks define candidate sets (nodes/edges) and target scores derived from exact or heuristic solves; these are specified in the task section.

### 3.2. Prescriptive tasks

Logistics planners face several classes of what-if queries, such as pre-commitment decisions (which deliveries to service vs. outsource) and post-commitment contingencies (how to respond to disruptions). We formalize two sensitivity tasks that capture these scenarios and are expensive to answer exactly, making them natural testbeds for learned representations.

**Node-removal sensitivity.** Consider an overloaded route that needs to drop one delivery. Removing a node cannot increase the length of the optimal tour, but some removals shorten it far more than others. Identifying the best node to remove is expensive, requiring a re-solve for each candidate. For labels, we remove each node  $i$ , re-solve to optimality, and record  $\Delta_i = L^*(X) - L^*(X \setminus \{i\})$  or its percent form.

**Edge-forbid sensitivity.** Now suppose a specific tour edge becomes unavailable due to a disruption such as a last-minute road closure. Forbidding an edge on the optimal tour adds a constraint, so the new optimal tour cannot be shorter. As with node-removal, measuring the impact of each tour edge requires  $n$  re-solves. We forbid each tour edge  $e$  in turn, re-solve to optimality, and record  $\Delta_e = L^*(\text{forbid } e) - L^*(X)$  (or its percent form).

Intuitively, edge-forbid impact depends on *replaceability*: an edge can be long yet easy to bypass if many near-equivalent alternatives exist, while a shorter “bridge” edge connecting sparse regions can be critical because forbidding it forces a different reconnection. This motivates our detour baseline, which cheaply estimates bypass quality using alternative paths.

### 3.3. Representation Extraction and Probing

**Collecting Activations.** For each checkpoint, we extract the policy encoder’s hidden representations and treat them as frozen features for probe training (architecture shown in Appendix A.1). We use the final encoder layer output (the last residual-stream activations), motivated by a layer-wise analysis showing that probe performance is stronger at the final layer than at intermediate layers and that this gap widens as training progresses (Appendix A.4). Because the encoder processes the entire graph in parallel, we do not need a full autoregressive rollout: a single for-

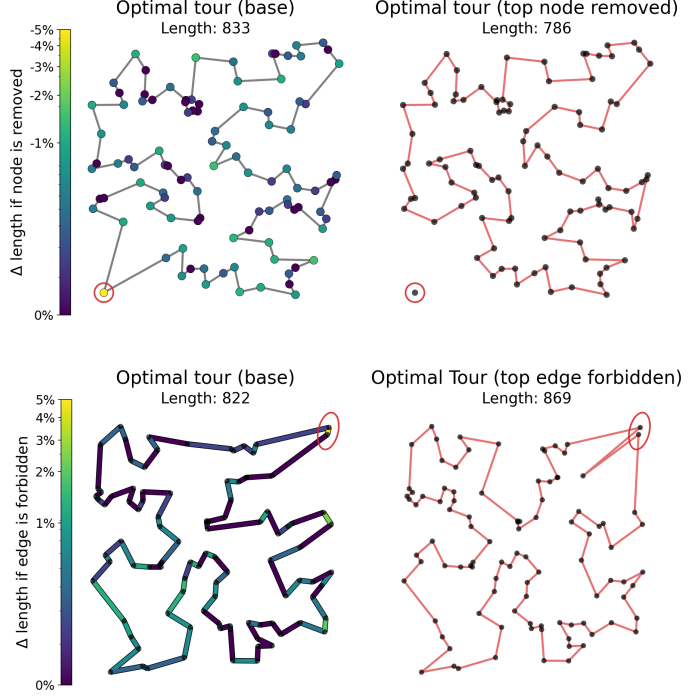


Figure 2. Sensitivity task examples on TSP100. **Top:** Base optimal tour with nodes colored by removal impact (left), and resulting tour after removing the best node (right, circled). **Bottom:** Base tour with edges colored by forbid impact (left), and resulting tour after forbidding the most critical edge (right, circled). Colors encode percent change in optimal tour length. Sensitivity depends on global structure, not local geometry.

ward pass suffices to extract per-node embeddings  $h_i \in \mathbb{R}^d$ . For node-removal tasks, we use node embeddings  $h_i$  directly; for edge-forbid tasks, we construct edge features from endpoint embeddings via concatenation with absolute difference:  $[h_u, h_v, |h_u - h_v|] \in \mathbb{R}^{3d}$ . Representations are extracted once per dataset and reused across all probe objectives and models.

**Candidate parameterization.** For node-removal, candidates are nodes, and the probe produces a scalar score for each node embedding  $h_i$ . For edge-forbid, we restrict candidates to the  $n$  edges on the optimal tour  $\pi^*$ . For tour position  $t$ , the candidate edge is  $(\pi_t^*, \pi_{t+1}^*)$ .

Each candidate edge  $(u, v)$  is represented using its endpoint embeddings via a symmetric feature map, concatenation of endpoints and their absolute difference  $[h_u, h_v, |h_u - h_v|]$ . Importantly, the probe scores edges using only their endpoint representations, without access to tour position or adjacency information.

This restriction to tour edges keeps the candidate set size  $O(n)$  (rather than  $O(n^2)$  over all edges) while matching the practical interdiction setting in which a currently used

connection becomes unavailable.

Concretely, for each checkpoint and dataset, we cache a tensor of per-node encoder outputs and associated candidate metadata (node indices or tour-edge pairs), and all probe training operates on these cached representations without re-running the TSP solver.

**Task labels** Ground-truth labels for both tasks require repeated optimal solves, which is computationally expensive but necessary for supervised probe training. For node-removal, we first solve the base instance to optimality with Concorde, then re-solve once for each node-removed. For a 100-node TSP instance, this requires 101 Concorde solves: one base solve plus 100 removal solves. The label for node  $i$  is the resulting  $\Delta_i$ , the reduction in optimal tour length when  $i$  is removed. Because the encoder preserves node order in its residual stream, each activation position along the sequence dimension corresponds to a specific node, allowing the probe to directly score and rank removals.

For edge-forbid, labels are defined relative to an optimal tour  $\pi^*$  of the base instance. Note, forbidding an edge that is not on the optimal tour would have no effect. We then perform  $n$  re-solves, each time forbidding one edge of  $\pi^*$  by setting its cost to a large value ( $10^7$ ), and record the resulting increase  $\Delta_e$  in optimal tour length. This restriction to tour edges keeps the candidate set at  $O(n)$  rather than  $O(n^2)$  over all possible edges.

In practice, edge-forbid labeling is substantially slower than node-removal: the Big- $M$  edge cost makes Concorde’s branch-and-cut search harder, resulting in re-solves that are approximately 3 times slower on average. For this reason, we use a smaller labeled dataset for edge-forbid (1000 instances) than for node-removal (3000 instances).

**Label generation.** We generate ground-truth sensitivity labels using Concorde. For node-removal, we write each instance to TSPLIB format with coordinate input, compute the base optimal tour length  $L^*(X)$ , then delete each node  $i$  in turn, re-solve to optimality, and record the percent improvement  $\Delta_i^{(\%)} = 100 \cdot \frac{L^*(X) - L^*(X \setminus \{i\})}{L^*(X)}$ , which is nonnegative since removing a node cannot increase the optimal tour length. For edge-forbid, we write Euclidean distances into an explicit distance matrix and forbid a tour edge by setting its symmetric costs  $D[u, v] = D[v, u] = C_{\text{forbid}}$  to  $C_{\text{forbid}} = 10^7$ , then re-solve to obtain:  $\Delta_e^{(\%)} = 100 \cdot \frac{L^*(X \mid \text{forbid } e) - L^*(X)}{L^*(X)}$ .

**Probe training.** We train a family of probes on frozen representations with controlled architectural capacity: linear models, DeepSets (MLP over sets), and Set Transformers, spanning simple linear readouts to expressive permutation-invariant set decoders. We evaluate multiple training objec-

tives (regression, hard CE, and soft/listwise CE) and observe tradeoffs between top- $k$  identification and rank correlation; objectives and hyperparameters are selected by validation performance. All probes operate on per-instance candidate sets and are trained without updating the frozen TSP solver. We use instance-level splits to avoid leakage: 2500/250/250 (train/val/test) for node-removal and 800/100/100 for edge-forbid. Input features are standardized using training-set statistics, and targets are standardized for regression objectives. Full configurations, hyperparameter sweeps, and objective ablations are in Appendix B.

### 3.4. Evaluation Metrics

For each instance, we score all candidates and take the target to be the argmax of  $\Delta$ . Our primary ranking metric is top- $k$  accuracy for  $k \in \{1, 5\}$  (whether the true best candidate appears in the top- $k$  predicted scores). We also report Spearman  $\rho$  between predicted scores and true  $\Delta$  within each instance; equivalently,  $\rho = \text{corr}(\text{rank}(\hat{s}), \text{rank}(\Delta)) = 1 - \frac{6 \sum_i d_i^2}{m(m^2 - 1)}$  with rank differences  $d_i$  over  $m$  candidates. Chance top- $k$  baselines are  $k/n$  for  $n$  candidates.

### 3.5. Computational cost of sensitivity labeling

A key motivation for representation-based predictors is computational. Exact labeling for both prescriptive tasks requires repeated optimal re-solves: for an instance with  $n$  nodes, both node-removal and edge-forbid require  $1 + n$  Concorde solves (one base solve plus one intervention solve per candidate). In contrast, a trained probe answers a query with a single encoder forward pass and a lightweight scoring network over candidates, without requiring any TSP re-solve at inference time.

To quantify the labeling burden in our setting, our dataset-collection pipeline logs wall-clock time for each Concorde call. On the datasets used in our main experiments, the end-to-end label-generation time per instance is substantial: node-removal labels average 18.9s per instance, and edge-forbid labels average approximately 49.6s per instance. These costs motivate our evaluation setting: we pay the labeling cost once to train probes, then amortize it into cheap inference-time rankings for what-if decision support.

This gap between expensive label generation and cheap encoder+probe inference makes representation-based sensitivity prediction attractive for decision support.

## 4. Experiments

### 4.1. Experimental Setup

We use a constructive TSP Attention Model policy in the style of (Kool et al., 2018) (RL4CO implementation). The encoder is a stack of Transformer blocks with residual con-

nections that contextualize each node embedding within the whole instance. The decoder is attention-based: conditioned on the encoded graph and the current tour state, it autoregressively selects the next node.

We train three model sizes (small/medium/full) by varying the residual-stream dimension (64/128/256), with 5 encoder layers and 8 attention heads. Training follows REINFORCE with a rollout baseline and gradient l2 clipping (clip value 10), using Adam with learning rate  $10^{-4}$  and exponential decay ( $\gamma = 0.998$ ). Instances are sampled on-the-fly from the uniform TSP100 distribution over  $[0, 1]^2$  in batches of 512, for 600k policy steps ( $\sim 300$ M rollouts total), and checkpoints are saved every 2000 steps for dynamics analyses. During training, we sample with a temperature of 0.5 and use greedy decoding during evaluation. Probe training always uses frozen checkpoints and does not require using the decoder.

## 4.2. Baselines and Controls

We design task-specific heuristics and deep-learning baselines to evaluate probe performance, along with controls that isolate what can be learned without access to solver representations. While the OR literature studies TSP reoptimization under node deletion and edge interdiction, we are not aware of standardized baselines for learning-based sensitivity ranking in our setting. We therefore define lightweight task-specific heuristics and non-probing deep-learning baselines, and include controls that isolate what the probe can learn without access to solver representations.

**Heuristic baselines.** For each task, we report two heuristic references under different query-time assumptions: a low-cost heuristic and a stronger tour-based heuristic. While node-removal naturally arises as *pre-solve* decision support and edge-forbid as *post-solve* contingency analysis, we include one of each style for both tasks as comparable reference points. Our low-cost heuristic does not require a tour solved to optimality (node-removal: tour-free geometry; edge-forbid: a closed-form score over edges of an available *base* tour), while the stronger heuristic assumes the *optimal* base tour is available and can be manipulated cheaply (node-removal: splice; edge-forbid: 2-opt repair).

*Node-removal (non-oracle).* We score each node by its nearest-neighbor distance  $s_i = \min_{j \neq i} \|x_i - x_j\|_2$  and predict  $\arg \max_i s_i$  (ties by index).

*Node-removal (oracle).* We include an *optimal-tour splice* baseline: given the optimal tour, remove node  $i$  and reconnect its predecessor and successor, scoring  $d(\text{prev}, i) + d(i, \text{next}) - d(\text{prev}, \text{next})$  (as a percent of the base optimal length), without additional local search (Archetti et al., 2003; Ausiello et al., 2009).

*Edge-forbid (non-oracle).* For edge-forbid, we use a *de-*

*tour* baseline that scores each candidate tour edge  $(u, v)$  by the best two-hop bypass via a third node,  $\Delta_{\text{detour}}(u, v) = \min_w [d(u, w) + d(w, v) - d(u, v)]$ , computed under the same distances used for labeling (Libura, 1991; Benchimol et al., 2010).

*Edge-forbid (oracle).* As a stronger reference, we use a 2-opt repair proxy: for each tour edge  $e$ , take the best feasible 2-opt swap that removes  $e$  and use the induced tour-length increase as an interdiction proxy (Croes, 1958; Johnson & McGeoch, 1997). See Appendix A.2 for full details.

**Deep-learning baselines (controls).** To test whether transfer is driven by probe capacity rather than information in solver representations, we use two controls (details in Appendix A.2). First, we train *representation-free* models that share the same decoder families as the probes (linear/DeepSets/transformer) but take only raw instance features (geometry-only). Second, we train the same probe families on activations from a randomly initialized encoder with identical architecture (random-init). Together, these controls quantify how far geometry-only learning can go and isolate the contribution of learning the TSP solver.

## 5. Results

### 5.1. Probe performance vs. baselines

Table 1 reports performance on node-removal and edge-forbid across three groups: lightweight heuristic baselines, representation-free ML baselines trained on raw instance inputs, and probes trained on frozen solver representations. For context, we also include two strong tour-based heuristics (splice for node-removal; 2-opt repair for edge-forbid) that assume access to an optimal tour of the base instance.

*Node-removal.* Among heuristic baselines, nearest-neighbor distance is already strong (0.440 top-1 / 0.857 top-5). A representation-free Set Transformer trained on raw instance inputs is the strongest non-tour baseline (0.577 top-1 / 0.873 top-5), suggesting that a permutation-invariant scorer on geometry can recover meaningful signal for this task. Probes on trained solver representations are competitive with, and slightly stronger than, geometry-only learning: our Set Transformer probe reaches 0.615 top-1 / 0.902 top-5.

For context, the tour-based splice heuristic is strong (0.630 top-1), but it assumes access to an optimal tour at inference. Our best reported ensemble instead remains non-tour: it combines the probe with the geometry-only Set Transformer via a convex combination of per-instance  $z$ -scored scores, improving to 0.653 top-1 / 0.933 top-5.

*Edge-forbid.* Edge-forbid is qualitatively different: a geometry-only Set Transformer trained on local edge-derived features performs poorly (0.14 top-1). As Figure 2 illustrates, interdiction impact depends on global structure

Table 1. Main transfer results on node-removal and edge-forbid. Top-1/top-5 report accuracy (whether the true best candidate appears in the model’s top-k predictions); Spearman is the rank correlation between predicted and ground-truth deltas. Ensemble combines probe scores with baseline features via learned convex combination.

Method	Node-removal			Edge-forbid		
	Top-1	Top-5	Spearman	Top-1	Top-5	Spearman
<i>Heuristic baselines</i>						
Heuristic baseline (nearest neighbor distance)	0.440	0.857	0.613	–	–	–
Detour baseline	–	–	–	0.540	0.940	0.668
Oracle tour, splice	0.630	0.790	<b>0.766</b>	–	–	–
Oracle tour, 2-opt repair	–	–	–	0.670	0.965	0.727
<i>ML baselines</i>						
Set-transformer, geometry-only	0.577	0.873	0.675	0.140	0.490	0.276
Linear probe, untrained policy	0.158	0.361	0.002	0.130	0.340	0.247
Transformer probe, untrained policy	0.503	0.835	0.597	0.220	0.562	0.383
<i>Probes</i>						
Linear probe	0.413	0.769	0.405	0.410	0.720	0.468
DeepSets probe	0.497	0.880	0.693	0.510	0.840	0.631
Transformer probe	0.615	0.902	0.736	0.462	0.818	0.626
Ensemble: transformer probe + geometry-only Set Transformer	<b>0.653</b>	<b>0.933</b>	0.739	–	–	–
Ensemble: transformer probe + 2-opt repair	–	–	–	<b>0.730</b>	<b>0.980</b>	<b>0.763</b>

rather than local edge geometry. In contrast, the non-oracle *detour* heuristic is already strong (0.540 top-1 / 0.940 top-5), since it incorporates a global bypass computation over alternative intermediate nodes. Probes substantially outperform representation-free deep baselines (0.462 top-1 / 0.818 top-5), partially closing the gap to the tour-based 2-opt repair baseline (0.670 top-1 / 0.965 top-5). As with node-removal, combining the probe with the oracle heuristic yields the best overall performance (0.73 top-1).

*Controls.* The random-initialized encoder controls show that performance is not explained solely by probe capacity: on edge-forbid, the transformer probe improves from 0.22 (untrained policy) to 0.462 (trained policy), indicating that learning to solve TSP induces task-relevant structure in the encoder. Overall, these results indicate that frozen neural TSP representations carry actionable signal for both prescriptive tasks, and probes can be competitive with strong non-oracle heuristics while surpassing oracle-at-inference baselines when combined with them.

## 5.2. Better Solvers Yield Better Probes

We measure solver quality by % suboptimality under greedy decoding on a fixed TSP100 validation set (Figure 3, top). For each saved checkpoint, we extract frozen encoder representations and train probes with a fixed configuration on the same downstream dataset splits, then report probe top-1 accuracy (Figure 3, bottom).

Table 2. Entries report Spearman  $\rho$  between probe top-1 accuracy and negative % suboptimality across saved checkpoints (every 2000 policy steps during training). Higher  $\rho$  indicates a more monotonic tendency for probe accuracy to increase as solver suboptimality decreases over training. Pooled row combines checkpoints from all 3 run sizes.

Model size	Node-removal		Edge-forbid	
	Linear	Transformer	Linear	Transformer
0.44M	0.77	-0.07	-0.45	0.01
1.10M	0.71	0.45	0.65	0.40
3.10M	0.83	0.61	0.59	0.32
All (pooled)	0.90	0.46	0.69	0.64

Across model sizes, the largest model (3.10M parameters) achieves both the lowest suboptimality and the strongest transfer on both tasks and probe families. Within each run, probe accuracy improved as the solver improved.

Table 2 reports correlation between TSP solver quality and probe accuracy. For most probe/task/policy combinations, higher solver quality strongly correlates with higher probe quality. The negative entries for the small model (edge-forbid, linear, and transformer probes) are driven by dynamics: accuracy improves sharply early, then plateaus with small late-stage declines, so the ranking is weakly anti-monotone even though absolute top-1 improves overall throughout training (from .19 to .26 for the linear probe and .19 to .245 for the transformer probe). Notably, the small

## Scaling: training vs probe accuracy

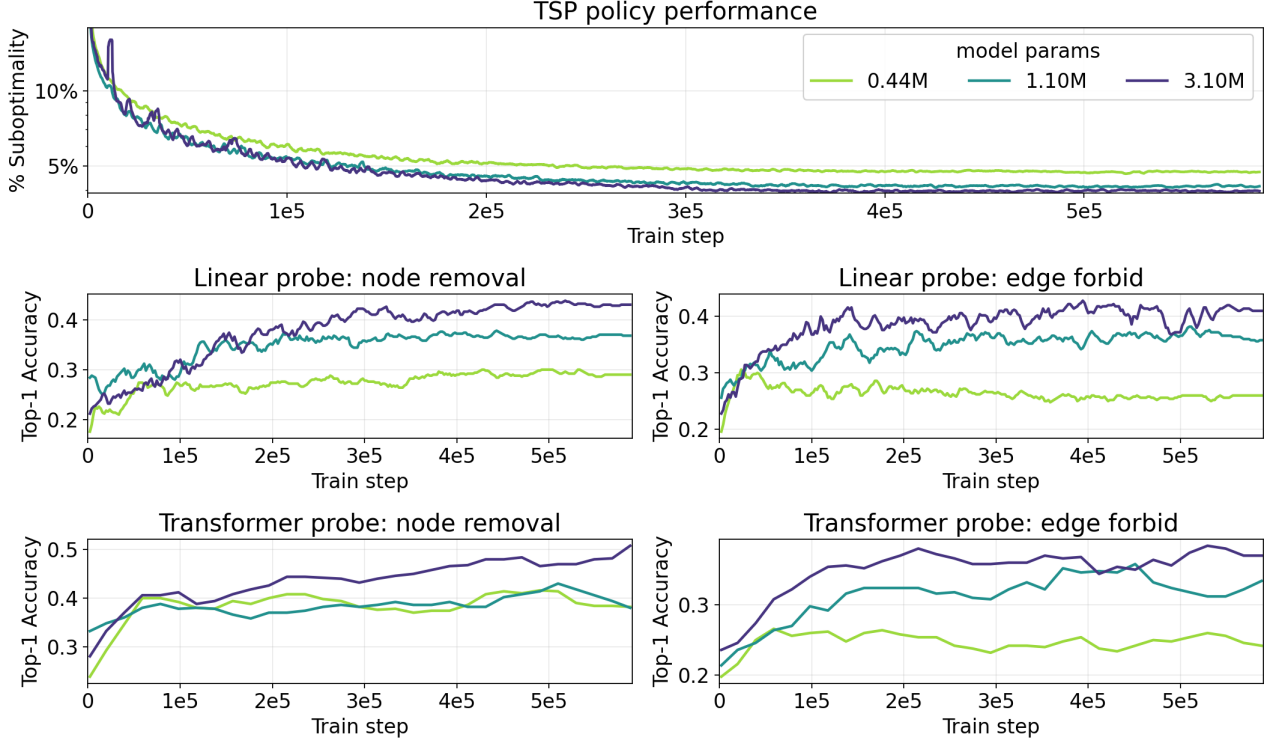


Figure 3. Training dynamics across model sizes. Top: TSP policy validation % suboptimality (greedy decoding) on a fixed TSP100 validation set. Bottom: probe top-1 accuracy across training checkpoints for node-removal and edge-forbid tasks, shown for linear and transformer probes trained on frozen encoder representations extracted at each checkpoint.

model’s transfer curves plateau earlier than the other models (Figure 3), reinforcing a well-known use case of probes as a practical diagnostic to monitor training dynamics (Nanda et al., 2023).

**Limitations and future work.** Our study focuses on Euclidean TSP100 and on sensitivity objectives defined relative to exact re-solves with Concorde. Extending to larger instances, richer routing constraints (e.g., time windows, capacities), or settings where exact labels are unavailable may require approximate labeling or different evaluation protocols. For edge-forbid, we restrict candidates to edges on the base optimal tour (to avoid an  $O(n^2)$  candidate set), so our results do not directly address interdiction over arbitrary edges. We also model forbiddance via a large Big- $M$  cost inflation, which is a standard proxy for unavailability but may not match all operational notions of disruption.

Finally, we use the AttentionModel architecture, which provides straightforward access to encoder representations for probe training. Stronger NCO solvers exist, such as POMO (Kwon et al., 2020). Testing whether these architectures yield even more transferable representations is a natural extension of our work.

## 6. Conclusion

Neural combinatorial optimization is typically evaluated as an end-to-end substitute for classical solvers: a policy is trained to construct tours, and success is measured by tour cost. This work addresses a complementary question: whether a trained neural TSP solver learns internal representations that transfer to *prescriptive* decision-support objectives beyond tour construction. We introduced two NP-hard sensitivity tasks, node-removal and edge-forbid, in which the goal is to rank small interventions by their effect on the *optimal* tour length. Across both tasks, probes trained on frozen encoder representations are competitive with strong non-representation baselines, and improve substantially over probes trained on random-initialized encoders. Moreover, transfer strengthens as the solver improves across training and model scale, suggesting that training stronger NCO solvers can yield more useful encoders for downstream what-if objectives. These findings suggest a broader value proposition for neural solvers: beyond inference-time tour quality, trained solvers can serve as reusable representations for related decision-support tasks.

## Impact Statement

This paper presents work whose goal is to advance the field of machine learning. There are many potential societal consequences of our work, none of which we feel must be specifically highlighted here.

## References

Applegate, D. L., Bixby, R. E., Chvátal, V., and Cook, W. J. *The Traveling Salesman Problem: A Computational Study*. Princeton University Press, Princeton, NJ, 2006. ISBN 978-0-691-12993-8. URL <https://press.princeton.edu/books/hardcover/9780691129938/the-traveling-salesman-problem>.

Archetti, C., Bertazzi, L., and Speranza, M. G. Reoptimizing the traveling salesman problem. *Networks*, 42(3):154–159, 2003. doi: 10.1002/net.10091. URL <https://doi.org/10.1002/net.10091>.

Ausiello, G., Escoffier, B., Monnot, J., and Paschos, V. T. Reoptimization of minimum and maximum traveling salesman’s tours. *Journal of Discrete Algorithms*, 7(4):453–463, 2009. doi: 10.1016/j.jda.2008.12.001. URL <https://doi.org/10.1016/j.jda.2008.12.001>.

Bello, I., Pham, H., Le, Q. V., Norouzi, M., and Bengio, S. Neural combinatorial optimization with reinforcement learning. *arXiv preprint arXiv:1611.09940*, 2016. URL <https://arxiv.org/abs/1611.09940>. Under review at ICLR 2017.

Benchimol, P., Régis, J.-C., Rousseau, L.-M., Rueher, M., and van Hoeve, W.-J. Improving the held and karp approach with constraint programming. In *Integration of AI and OR Techniques in Constraint Programming for Combinatorial Optimization Problems (CPAIOR 2010)*, volume 6140 of *Lecture Notes in Computer Science*, pp. 40–44. Springer, 2010. doi: 10.1007/978-3-642-13520-0\_6. URL [https://doi.org/10.1007/978-3-642-13520-0\\_6](https://doi.org/10.1007/978-3-642-13520-0_6).

Bengio, Y., Lodi, A., and Prouvost, A. Machine learning for combinatorial optimization: a methodological tour d’horizon. *arXiv preprint arXiv:1811.06128*, 2018. URL <https://arxiv.org/abs/1811.06128>. European Journal of Operational Research, 2021 (journal version).

Berto, F., Hua, C., Park, J., Luttmann, L., Ma, Y., Bu, F., Wang, J., Ye, H., Kim, M., Choi, S., Gast Zepeda, N., Hottung, A., Zhou, J., Bi, J., Hu, Y., Liu, F., Kim, H., Son, J., Kim, H., Angioni, D., Kool, W., Cao, Z., Zhang, Q., Kim, J., Zhang, J., Shin, K., Wu, C., Ahn, S., Song, G., Kwon, C., Tierney, K., Xie, L., and Park, J. RL4CO: an extensive reinforcement learning for combinatorial optimization benchmark. *arXiv preprint arXiv:2306.17100*, 2023. URL <https://arxiv.org/abs/2306.17100>. KDD 2025 Oral.

Berto, F., Hua, C., Gast Zepeda, N., Hottung, A., Wouda, N., Lan, L., Park, J., Tierney, K., and Park, J. Routefinder: Towards foundation models for vehicle routing problems. *arXiv preprint arXiv:2406.15007*, 2024. doi: 10.48550/arXiv.2406.15007. URL <https://arxiv.org/abs/2406.15007>. TMLR 2025.

Cappart, Q., Chételat, D., Khalil, E. B., Lodi, A., Morris, C., and Veličković, P. Combinatorial optimization and reasoning with graph neural networks. *arXiv preprint arXiv:2102.09544*, 2021. URL <https://arxiv.org/abs/2102.09544>.

Croes, G. A. A method for solving traveling-salesman problems. *Operations Research*, 6(6):791–812, 1958. doi: 10.1287/opre.6.6.791.

Gireesan, G., Pillai, N., Rothrock, M. J., Nanduri, B., Chen, Z., and Ramkumar, M. Deep sensitivity analysis for objective-oriented combinatorial optimization. *arXiv preprint arXiv:2403.00016*, 2024. URL <https://arxiv.org/abs/2403.00016>.

Goh, Y. L., Cao, Z., Ma, Y., Zhou, J., Dupuy, M. H., and Lee, W. S. Shield: Multi-task multi-distribution vehicle routing solver with sparsity and hierarchy. In *International Conference on Machine Learning (ICML)*, 2025. URL <https://openreview.net/forum?id=6DJEaz1cCj>. OpenReview.

Hewitt, J. and Liang, P. Designing and interpreting probes with control tasks. *arXiv preprint arXiv:1909.03368*, 2019. URL <https://arxiv.org/abs/1909.03368>. EMNLP 2019.

Hewitt, J. and Manning, C. D. A structural probe for finding syntax in word representations. In *Proceedings of NAACL-HLT*, 2019. doi: 10.18653/v1/N19-1419. URL <https://aclanthology.org/N19-1419/>.

Hudson, B., Li, Q., Malencia, M., and Prorok, A. Graph neural network guided local search for the traveling salesperson problem. *arXiv preprint arXiv:2110.05291*, 2021. URL <https://arxiv.org/abs/2110.05291>. ICLR 2022.

Johnson, D. S. and McGeoch, L. A. The traveling salesman problem: A case study in local optimization. In Aarts, E. H. L. and Lenstra, J. K. (eds.), *Local Search in Combinatorial Optimization*, pp. 215–310. John Wiley & Sons, London, UK, 1997. URL <https://doi.org/10.1002/9780470316006.ch10>.

[www.cs.ubc.ca/~hutter/previous-earg/EmpAlgReadingGroup/TSP-JohMcg97.pdf](http://www.cs.ubc.ca/~hutter/previous-earg/EmpAlgReadingGroup/TSP-JohMcg97.pdf).

Joshi, C. K., Cappart, Q., Rousseau, L.-M., and Laurent, T. Learning the travelling salesperson problem requires rethinking generalization. *arXiv preprint arXiv:2006.07054*, 2020. URL <https://arxiv.org/abs/2006.07054>.

Kool, W., van Hoof, H., and Welling, M. Attention, learn to solve routing problems! *arXiv preprint arXiv:1803.08475*, 2018. URL <https://arxiv.org/abs/1803.08475>. ICLR 2019.

Kwon, Y.-D., Choo, J., Kim, B., Yoon, I., Gwon, Y., and Min, S. POMO: Policy optimization with multiple optima for reinforcement learning. *arXiv preprint arXiv:2010.16011*, 2020. URL <https://arxiv.org/abs/2010.16011>.

Lee, J., Lee, Y., Kim, J., Kosiorek, A., Choi, S., and Teh, Y. W. Set transformer: A framework for attention-based permutation-invariant neural networks. In *Proceedings of the 36th International Conference on Machine Learning*, volume 97 of *Proceedings of Machine Learning Research*, pp. 3744–3753. PMLR, 2019. URL <https://proceedings.mlr.press/v97/lee19d.html>.

Li, J., Chen, W., and Guo, M. Neural tractability via structure: Learning-augmented algorithms for graph combinatorial optimization. *arXiv preprint arXiv:2511.19573*, 2025. URL <https://arxiv.org/abs/2511.19573>.

Libura, M. Sensitivity analysis for minimum hamiltonian path and traveling salesman problems. *Discrete Applied Mathematics*, 30(2–3):197–211, 1991. doi: 10.1016/0166-218X(91)90044-W. URL [https://doi.org/10.1016/0166-218X\(91\)90044-W](https://doi.org/10.1016/0166-218X(91)90044-W).

Lin, S. and Kernighan, B. W. An effective heuristic algorithm for the traveling-salesman problem. *Operations Research*, 21(2):498–516, 1973. doi: 10.1287/opre.21.2.498.

Liu, F., Lin, X., Wang, Z., Zhang, Q., Tong, X., and Yuan, M. Multi-task learning for routing problem with cross-problem zero-shot generalization. *arXiv preprint arXiv:2402.16891*, 2024. doi: 10.48550/arXiv.2402.16891. URL <https://arxiv.org/abs/2402.16891>.

Lozano, L., Smith, J. C., and Kurz, M. E. Solving the traveling salesman problem with interdiction and fortification. In *Operations Research Letters*, volume 45, pp. 210–216, 2017. doi: 10.1016/j.orl.2017.02.007. URL <https://www.sciencedirect.com/science/article/abs/pii/S0167637717301098>.

Ma, Y., Li, J., Cao, Z., Song, W., Zhang, L., Chen, Z., and Tang, J. Learning to iteratively solve routing problems with dual-aspect collaborative transformer. *arXiv preprint arXiv:2110.02544*, 2021. URL <https://arxiv.org/abs/2110.02544>. NeurIPS 2021.

Nanda, N., Chan, L., Lieberum, T., Smith, J., and Steinhardt, J. Progress measures for grokking via mechanistic interpretability. *arXiv preprint arXiv:2301.05217*, 2023. doi: 10.48550/arXiv.2301.05217. URL <https://arxiv.org/abs/2301.05217>.

Narad, R., Boussioux, L., and Wagner, M. Mechanistic interpretability for neural TSP solvers. *arXiv preprint arXiv:2510.21693*, 2025. URL <https://arxiv.org/abs/2510.21693>. NeurIPS 2025 MLxOR Workshop.

Nazari, M., Oroojlooy, A., Snyder, L. V., and Takáč, M. Reinforcement learning for solving the vehicle routing problem. *arXiv preprint arXiv:1802.04240*, 2018. URL <https://arxiv.org/abs/1802.04240>.

Vinyals, O., Fortunato, M., and Jaitly, N. Pointer networks. *arXiv preprint arXiv:1506.03134*, 2015. URL <https://arxiv.org/abs/1506.03134>.

Yuan, H., Ouyang, W., Zhang, C., Li, C., and Sun, Y. OPTFM: A scalable multi-view graph transformer for hierarchical pre-training in combinatorial optimization. OpenReview (NeurIPS 2025 Spotlight), 2025. URL <https://openreview.net/forum?id=24tuzE5KZc>.

Zaheer, M., Kottur, S., Ravanbakhsh, S., Poczos, B., Salakhutdinov, R. R., and Smola, A. J. Deep sets. In *Advances in Neural Information Processing Systems 30*, pp. 3391–3401. Curran Associates, Inc., 2017. URL <https://papers.nips.cc/paper/6931-deep-sets>.

Zhang, L., Chen, Z., Lu, C.-T., and Zhao, L. Network interdiction goes neural. *arXiv preprint arXiv:2405.16409*, 2024. URL <https://arxiv.org/abs/2405.16409>. KDD 2025.

Zhang, Z., Ma, Y., Cao, Z., and Lau, H. C. Probing neural combinatorial optimization models. *arXiv preprint arXiv:2510.22131*, 2025a. URL <https://arxiv.org/abs/2510.22131>. Accepted as Spotlight at NeurIPS 2025.

Zhang, Z., Ma, Y., Yang, J., Cao, Z., and Lau, H. C. Unveiling neural combinatorial optimization model representations through probing. OpenReview (Submitted to ICLR 2025), 2025b. URL <https://openreview.net/forum?id=agEy9hliY1>.

Zhou, J., Cao, Z., Wu, Y., Song, W., Ma, Y., Zhang, J., and Xu, C. Mvmoe: Multi-task vehicle routing solver with mixture-of-experts. In *Proceedings of the 41st International Conference on Machine Learning*, volume 235 of *Proceedings of Machine Learning Research*, pp. 61804–61824. PMLR, 2024. URL <https://proceedings.mlr.press/v235/zhou24c.html>.

## A. Method and baseline details

### A.1. Representation extraction

We treat a trained neural TSP solver as a frozen encoder that maps an instance  $X = \{x_i\}_{i=1}^n$  to contextualized node representations  $H = \{h_i\}_{i=1}^n$ ,  $h_i \in \mathbb{R}^d$ . In all experiments, we extract representations from the tensor returned by the RL4CO AttentionModel encoder (the final encoder output after the full stack), with shape  $[B, n, d]$  for a batch of  $B$  instances. Our extraction applies no additional projection or normalization at extraction time; standardization (when used) is applied during probe training.

**Candidate mapping and edge features.** For node-removal sensitivity, the candidate set is the set of nodes. Each node  $i$  corresponds directly to one representation  $h_i$ , and a probe produces a scalar score per node.

For edge-forbid sensitivity, the candidate set is restricted to the  $n$  edges on an optimal tour  $\pi^*$ . For tour position  $t \in \{1, \dots, n\}$  (with wrap-around), the candidate edge is  $(u, v) = (\pi_t^*, \pi_{t+1}^*)$ . We form an edge feature vector from endpoint representations via

$$x_{uv} = [h_u, h_v, |h_u - h_v|] \in \mathbb{R}^{3d},$$

and the probe produces a scalar score per tour edge. The ordering of  $(u, v)$  follows the tour direction (it is not symmetrized, except for the  $|h_u - h_v|$  term).

**Caching.** Representations are cached once per checkpoint and dataset and reused across probe runs. This decouples expensive representation extraction from probe training and ensures that probes compare downstream decoder choices while holding encoder features fixed.

### A.2. Baselines

This section specifies the baselines used in Table 1. We distinguish non-tour baselines (which use only instance geometry) from tour-based baselines (which assume access to an optimal tour of the base instance).

**Node-removal: nearest-neighbor heuristic (non-tour).** For each node  $i$ , define the nearest-neighbor distance score

$$s_i = \min_{j \neq i} \|x_i - x_j\|_2.$$

We predict the best node to remove as  $\arg \max_i s_i$  (ties broken by index order).

**Node-removal: splice heuristic (tour-based).** Given an optimal tour  $\pi^*$ , let  $\text{prev}(i)$  and  $\text{next}(i)$  denote the tour neighbors of node  $i$ . We score node  $i$  by the immediate shortcut improvement obtained by removing  $i$  from the tour and reconnecting its neighbors:

$$s_i = d(\text{prev}(i), i) + d(i, \text{next}(i)) - d(\text{prev}(i), \text{next}(i)).$$

We evaluate this score in percent-of-base-length units to match the label convention.

**Edge-forbid: detour heuristic (non-tour).** For each candidate tour edge  $(u, v)$ , we score its *detour cost* by the best two-hop bypass through a third node:

$$s_{uv} = \min_{w \notin \{u, v\}} [d(u, w) + d(w, v) - d(u, v)].$$

Larger values indicate that forbidding  $(u, v)$  is likely to force a larger increase in tour length. Distances are computed using the same discretized metric used for Concorde labeling.

**Edge-forbid: 2-opt repair proxy (tour-based).** Given an optimal tour  $\pi^*$ , consider a candidate tour edge  $e = (A_i, B_i)$  and a second tour edge  $(A_j, B_j)$  that is not adjacent to  $e$  on the tour. The standard 2-opt move removes both edges and reconnects the tour in one of two ways, with induced length changes:

$$\begin{aligned} \Delta_1 &= d(A_i, A_j) + d(B_i, B_j) - d(A_i, B_i) - d(A_j, B_j), \\ \Delta_2 &= d(A_i, B_j) + d(B_i, A_j) - d(A_i, B_i) - d(A_j, B_j). \end{aligned}$$

We score edge  $e$  by the best (smallest) feasible 2-opt increase over all non-adjacent choices:

$$s_e = \max \left( 0, \min_j \min \{ \Delta_1, \Delta_2 \} \right),$$

where the max clamps negative values to 0. This provides a fast tour-based proxy for interdiction impact.

**Geometry-only deep baselines.** We also train representation-free deep baselines using the same probe decoder family, but with geometry-only inputs. For node-removal, each node is represented by  $(x_i, y_i, \text{mn\_dist}_i)$ . For edge-forbid, each tour-edge candidate is represented by endpoint-derived features including  $(x_u, y_u, x_v, y_v)$ , differences  $(\Delta x, \Delta y)$ , and distance-based scalars (e.g.,  $\|\Delta\|_2$  and elementwise absolute differences).

**Random-init control.** We repeat probe experiments using activations extracted from a randomly initialized policy encoder with identical architecture. This keeps the representation interface fixed while removing learned structure, isolating the contribution of training the TSP solver.

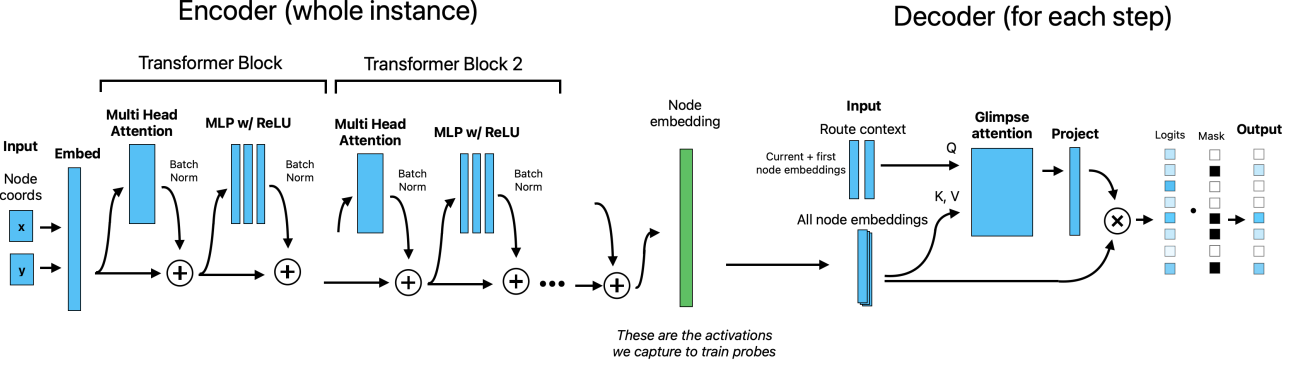


Figure 4. AttentionModel architecture (encoder/decoder). We cache the final encoder output (encoder\_output) as frozen node representations for probing; the decoder is not used for representation extraction.

**Ensembles.** For node-removal, the reported non-tour ensemble combines probe scores with the geometry-only deep baseline using a convex combination of per-instance  $z$ -scored scores, with the mixing weight selected on the validation set. For edge-forbid, the reported ensemble combines probe scores with the tour-based 2-opt proxy using a convex combination of raw scores, again selecting the mixing weight on the validation set.

### A.3. Probe architectures and objectives

All probes operate on a candidate set for a single instance and output one scalar score per candidate.

**Linear probe.** A linear probe maps each candidate feature vector  $x_i$  (node embedding or edge feature) to a score  $s_i = w^\top x_i + b$ .

**DeepSets probe.** DeepSets (Zaheer et al., 2017) parameterize a permutation-invariant scorer by combining a per-element network and a pooled context. Given candidate features  $x_i$ , we compute:

$$h_i = \phi(x_i), \quad \bar{h} = \frac{1}{m} \sum_{j=1}^m h_j, \quad s_i = \rho([h_i, \bar{h}]),$$

where  $m$  is the number of candidates and  $\phi, \rho$  are MLPs. We use mean pooling (with masking when appropriate).

**Transformer probe.** Our strongest probe uses a permutation-equivariant Transformer encoder without positional embeddings. Given a sequence of candidate features  $\{x_i\}_{i=1}^m$ , a TransformerEncoder maps them to contextualized outputs  $\{z_i\}_{i=1}^m$ , and a shared linear head produces scores  $s_i = w^\top z_i + b$ . Note that this is a plain TransformerEncoder used in a set setting; it is related in spirit to Set Transformer (Lee et al., 2019) but does not use the SAB/ISAB/PMA modules.

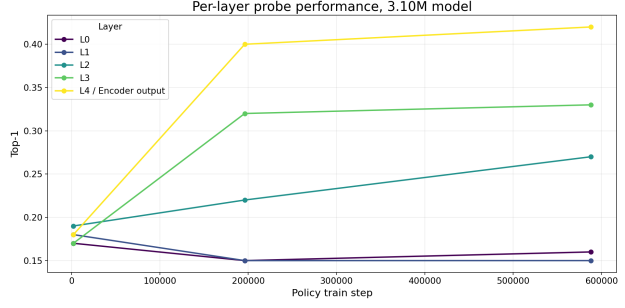


Figure 5. Layer-wise probeability across training for a linear probe (top-1 accuracy). Curves correspond to encoder block outputs (encoder\_layer\_0–encoder\_layer\_4) and the final encoder output (encoder\_output).

**Objectives.** Hard cross-entropy uses the argmax- $\Delta$  candidate as the class label. Soft cross-entropy uses a target distribution over candidates  $p_i \propto \exp(\Delta_i/\tau)$  (with temperature  $\tau$ ) and minimizes cross-entropy between  $p$  and the model scores. Regression uses Mean Squared Error (MSE) on the percent-delta targets.

### A.4. Layer sweep

This section supports the choice to probe the final encoder output. Figure 5 shows a layer-wise probeability analysis for a fixed linear probe configuration evaluated across training checkpoints. Later layers become increasingly probeable over training, and the final encoder output is consistently the strongest choice. We therefore use the final encoder output throughout the main experiments.

## B. Probe configurations and hyperparameter selection

This section documents the probe configurations and selection procedure used for the results in Table 1. Unless otherwise stated, we use frozen activations extracted from

Table 3. Objective ablations (single seed). Metrics are Top-1 / Top-5 / Spearman.

Node-removal	
Linear (reg)	0.307 / 0.713 / 0.565
Linear (hard CE)	0.417 / 0.787 / 0.400
Linear (soft CE)	0.343 / 0.763 / 0.533
DeepSets (reg)	0.503 / 0.877 / 0.704
DeepSets (hard CE)	0.470 / 0.843 / 0.504
DeepSets (soft CE)	0.523 / 0.860 / 0.696
Transf. (reg)	0.557 / 0.897 / 0.728
Transf. (hard CE)	0.430 / 0.770 / 0.465
Transf. (soft CE)	0.523 / 0.897 / 0.722
Edge-forbid	
Linear (reg)	0.410 / 0.750 / 0.552
Linear (hard CE)	0.410 / 0.680 / 0.456
Linear (soft CE)	0.400 / 0.740 / 0.548
DeepSets (reg)	0.450 / 0.850 / 0.639
DeepSets (hard CE)	0.410 / 0.700 / 0.472
DeepSets (soft CE)	0.410 / 0.830 / 0.636
Transf. (reg)	0.420 / 0.820 / 0.645
Transf. (hard CE)	0.400 / 0.700 / 0.406
Transf. (soft CE)	0.510 / 0.830 / 0.621

the final checkpoint of the full expdecay policy.

**Splits and preprocessing.** Node-removal uses a fixed 2500/250/250 instance split (train/val/test); edge-forbid uses 800/100/100. For all probes and baselines, we standardize input features  $X$  using train-set statistics. For regression probes, we standardize targets  $y$  using the train-set mean and standard deviation, and unstandardize for reporting.

**Hyperparameter selection.** For node-removal we sweep probe families (linear, DeepSets, transformer) and objectives (regression MSE, hard CE, soft CE), selecting by validation loss (regression) or validation top-1 (classification). Linear probes are reported as 20-seed means; transformer probes are reported as 5-seed means. For edge-forbid we sweep transformer objectives and temperatures (soft-CE  $\tau \in \{0.5, 1, 2\}$ ), learning rates (3e-4, 1e-3), and transformer width/depth, selecting by validation loss; results are reported as 5-seed means unless noted. Training uses AdamW for 50 epochs with the batch sizes listed in the experiment configs.

**Objective ablations (single-seed).** Table 3 compares regression vs. hard/soft cross-entropy objectives for linear, DeepSets, and Transformer probes on each task (single seed; fixed splits;  $\tau = 2$  for soft CE).

### Best configurations (Table 1).

- Linear probe (node-removal): regression (MSE) on  $\Delta^{(\%)}$ , lr 1e-2, weight decay 0; 20-seed mean.
- Linear probe (edge-forbid): soft cross-entropy on  $\Delta^{(\%)}$

with fixed temperature, lr 1e-2, weight decay 0; 5-seed mean.

- DeepSets probe (node-removal): regression (MSE), hidden dim 256, 2 layers, dropout 0.1, lr 1e-3, weight decay 1e-4; selected by val loss.
- DeepSets probe (edge-forbid): soft-CE with  $\tau = 2$ , hidden dim 256, 3 layers, dropout 0.1, lr 1e-3, weight decay 1e-3; selected by val loss.
- Transformer probe (node-removal): regression (MSE),  $d = 256$ , 4 layers, 4 heads, ff=512, dropout 0.1, lr 3e-4, weight decay 1e-3; 5-seed mean.
- Transformer probe (edge-forbid): soft-CE with  $\tau = 2$ ,  $d = 256$ , 4 layers, 4 heads, ff=512, dropout 0.1, lr 1e-3, weight decay 1e-3; 5-seed mean.
- Geometry-only Set Transformer (node-removal): trained on  $(x_i, y_i, \text{nn.dist}_i)$  features with the same transformer hyperparameters as above where applicable.
- Geometry-only Set Transformer (edge-forbid): trained on endpoint-derived edge features as described in Appendix A.2.
- Ensemble (node-removal): convex combination of per-instance  $z$ -scored scores from transformer probe and geometry-only baseline;  $\alpha \in \{0, 0.1, \dots, 1\}$  selected by val top-1.
- Ensemble (edge-forbid): convex combination of raw scores from transformer probe and 2-opt baseline;  $\alpha \in \{0, 0.1, \dots, 1\}$  selected by val top-1.
- Random-init controls: same probe families and hyperparameters as above, using activations from a randomly initialized encoder (see Appendix A.2).